TÜBİTAK

Turkish Journal of Engineering & Environmental Sciences

http://journals.tubitak.gov.tr/engineering/

Research Article

Turkish J Eng Env Sci
(2014) 38: 97 – 111

doi:10.3906/muh-1308-11

Variations in clear water scour geometry at piers of different effective widths

Subhasish DAS*, Rajib DAS, Asis MAZUMDAR
School of Water Resources Engineering, Jadavpur University, Kolkata, West Bengal, India

Received: 17.08.2013 • **Accepted:** 05.08.2014 • **Published Online:** 24.10.2014 • **Printed:** 21.11.2014

Abstract: The equilibrium scour geometry around a circular pier protruding vertically on a scoured channel bed was experimentally investigated. In order to conduct a comparative study, measurements within an equilibrium scour hole at a square pier, an equilateral triangular pier, and a flat plate with sides, facing the approaching flow, equaling the width of the circular pier were taken. Flow in an equilibrium scour hole under a clear water regime was considered for 4 separate tests. Tests were carried out for approaching flow having undisturbed constant flow depth greater than the pier width with a depth-averaged approaching flow velocity of about 68.2% representing the critical velocity of the uniform sand bed. It was observed that all the equilibrium dimensionless scour parameters, namely scour depth, length, width, area, and volume, depend on the effective pier width equal to the diameter of the smallest circumscribing circle of the pier. When the effective pier diameter increases and approaching flow depth is constant, scour parameters increase. Based on the results, some empirical equations are proposed for the scour depth, scour length, scour width, scour area, and scour volume. These equations may be utilized to estimate scour geometry in future studies.

Key words: Open channel flow, pier, flat plate, scour, sediment transport

1. Introduction

Scour is a natural phenomenon of lowering the level of riverbeds by the erosive action of the flowing stream. The amount of reduction in the level of riverbeds below an assumed natural level is termed scour depth. Local scour (also termed localized scour) develops near the structures, due to modification of the flow field as a result of obstruction to the flow by the structures. Scour at bridge piers is an example of local scour. Local scour, sometimes called clear-water scour, occurs when the sediment is removed from the scour hole but not supplied by the approaching stream. The equilibrium scour depth is attained when the fluid induced force can no longer dislodge the sediment particles from the scour hole.

Failure of bridges due to scour at their supports is a common occurrence. It may be due to scour at a pier or at an abutment. Major scouring usually occurs during floods, that is, when the flow is unsteady and may even have a changed angle relative to low flow direction. The problem is often further complicated by the large variety of shapes and approaches used for piers and abutments. Chabert and Engeldinger [1] appear to have been the first to describe the behavioral pattern of scour at a circular pier in terms of development with time and flow velocity.

Several investigations have been carried out with the purpose of predicting scour and various equations have been developed [2–21]. The formulae give widely differing estimates. These disparities have been discussed

*Correspondence: subhasishju@gmail.com

by many researchers [22–24]. Futhermore, to check the accuracy of the developed scour equations, comparative studies have been carried out [25–27].

The pier diameter (b) relative to the mean bed particle size (d_{50}) is known as the sediment coarseness (b/d_{50}). The equilibrium scour depth decreases with decreasing sediment coarseness for values less than about 20 to 25. It also decreases at a greater rate with decreasing flow depth for smaller values of flow shallowness or relative inflow depth, h/b (where h is the approaching flow depth), which is one of the main parameters influencing local scour. It was indicated that the relative scour depth (d_{se}/b) is a function of flow shallowness, where d_{se} is the equilibrium depth of local scour [28]. The author presented a relationship between d_{se}/b and h/b through curves. Earlier, such curves were developed by a number of researchers [5,29–32].

Later the researchers presented a scour equation and found that densimetric Froude number is the dominant parameter governing the scour process [33]. The proposed equation for temporal scour evolution was further justified with a large set of experimental results [34]. Temporal variation in dimensionless scour area and volume has also been reported and empirical relationships were developed [35]. Recently experiments were conducted [36] to find out the vorticity and circulation of a horseshoe vortex in equilibrium scour holes at a circular pier, square pier, and equilateral triangular pier (sides facing the approaching flow) of the same width but different effective width. It was observed that the circulation increases if the effective pier width or the effective obstruction width of the pier increases for the equilibrium scour condition. It indicates that effective pier width is also an important factor for scour analysis. However, it appears from our literature survey that almost no experimental work has been carried out to study the scour geometry within scour holes located around different shaped piers of the same width but different effective pier width. In spite of the large number of investigations focusing on single piers, a comprehensive understanding of the scour geometry for single piers is still deficient because most of the popular empirical equations were based on pier width only; hence, the consequences of effective pier width are lacking.

The present study reports the clear water scour geometry analysis at equilibrium scour condition around a circular pier, square pier, equilateral triangular pier, and flat plate (sides facing the approaching flow) of the same width but different effective pier width.

2. Experimental apparatus and program

In the present work, investigation of scour depth and measurement of velocity by acoustic Doppler velocimeter (ADV) was carried out. The experimental setup of the work is described in detail with the help of the schematic diagram shown in Figures 1a–1d. All the experiments (tests) were conducted in the Fluvial Hydraulics Laboratory of the School of Water Resources Engineering at Jadavpur University in Kolkata, West Bengal, India.

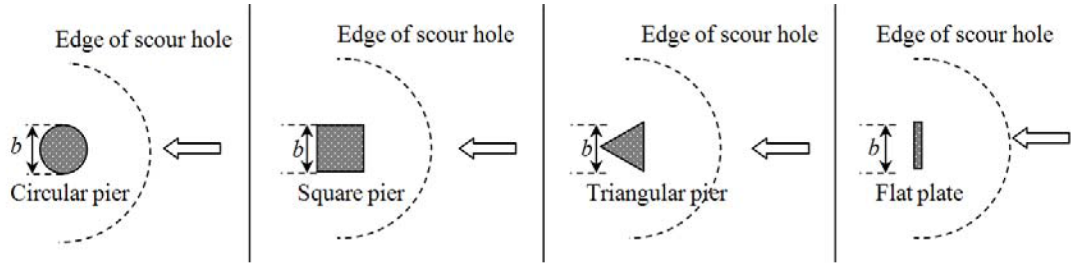

Figure 1. Horizontal planes of scour holes for (a) circular pier, (b) square pier, (c) equilateral triangular pier, and (d) flat plate.

The experiments were carried out in a re-circulating tilting flume 11-m long, 0.81-m wide, and 0.60-m deep. The working section of the flume was filled with sand to a uniform thickness of 0.20 m; the length of the sand bed was 3 m and the width was 0.81 m. The sand bed was located 2.9 m upstream from the flume inlet. Table 1 summarizes the experimental conditions of all the tests planned for this research.

Table 1. Experimental condition for all tests.

Test no.	b (cm)	Q (L/s)	h (cm)	Pier shape	φ_r (^{o})	F (-)	u_c (m/s)	R_e (-)	R_p (-)
1	11	25	12.5	Circular	40.53	0.223	0.362	24165	27828
2	11	25	12.5	Square	40.09	0.223	0.362	24165	27828
3	11	25	12.5	Triangular	40.73	0.223	0.362	24165	27828
4	11	25	12.5	Flat plate	41.05	0.223	0.362	24165	27828

Note: Q is the discharge; u_c is the critical velocity; φ_r is the dynamic angle of repose; F is the Froude number and R_e is the flow Reynolds number.

The re-circulating flow system was served by a 10-hp variable speed centrifugal pump located at the upstream end of the tilting flume. The rpm of the pump was 1450 with a power of 7.5 kW and a maximum discharge of 25.5 L/s. The water discharge was measured by a flowmeter connected to the upstream pipe at the inlet of the flume. Water flows through a 0.2-m-diameter pipe line, which runs directly into the flume. A movable trolley with a point gauge attached to it was positioned on the flume. A vertical scale was fixed with the point gauge to measure the water level, initial bed level, and scour depth. Piers were placed in the middle of the working section of the flume. During the tests, it was kept in mind that the width of the experimental flume is more than 6.25 times that of the pier width to avoid the wall friction factor as proposed by Raudkivi and Ettema [8].

All tests were conducted using one bed material. The bed material (sand particles) size was d_{50} (= 0.825 mm), d_{16} (= 0.5 mm), d_{84} (= 1.62 mm), and d_{90} (= 1.78 mm), measured from the sieve analysis test using a vibrating shaker. Geometric standard deviation of sand particle size, σ_g, given by $\sqrt{d_{84}/d_{16}}$, was equal to 1.8. Relative density of the sand (s), angle of repose of the bed sediment in still water (φ), average bed shear stress, and critical bed shear stress were 2.582, 36°, 0.39 Pa, and 0.40 Pa, respectively. The dynamic angle of repose (φ_r) was about 13% greater than the φ, whereas it was about 15% as observed previously [37,38]. The critical condition of the bed was checked before each test run as recommended [39].

The flow depth in the flume was adjusted by a tailgate. The mean approaching flow depth (h) was maintained as 0.125 m by operating the tailgate. The bed slope, equal to 1:2400, was kept constant for all tests. All tests were conducted for the approaching flow having undisturbed flow depth where the ratio between the approach flow depth and pier width (b) was 1.14. The depth-averaged approaching flow velocity (U) was set as 0.247 m/s, which is about 68.2% of the critical velocity (u_c) to satisfy the clear water condition, i.e. the present study considered only clear water approach flow conditions described by a velocity ratio $U/u_c = 0.682$ [33,40]. The section averaged approaching flow velocity was determined from the measured vertical profile of the approaching flow velocity 2 m upstream from the pier where the presence of the pier did not affect the approaching flow.

When negligible (1 mm or less) difference of scour depth was observed at an interval of 2 h after 72 h, it was considered that an equilibrium stage of the scour hole had been attained. However, total duration of each experiment was 80 h, which was adequate for achieving the equilibrium scour [41,42]. After the run was ended,

the maximum equilibrium scour depth was observed at the upstream base of the pier. Then the maximum scour depth at an equilibrium state was carefully measured by a Vernier point gauge with an accuracy of ± 0.1 mm.

3. Analyses of equilibrium scour geometry

The scour affected zones and contour lines of the scour holes at the circular pier, square pier, equilateral triangular pier, and flat plate, plotted with the Golden software Surfer version 8.06.39, are shown in Figures 2a–2d and Figures 3a–3d, respectively. Here scours are slightly asymmetric due to some local effects. Table 2 summarizes the values obtained for scour parameters for all tests. In Table 2, the values of planner surface area (a_{se}) and volume (v_{se}) of the equilibrium scour holes were estimated with the help of gauged data and Surfer software.

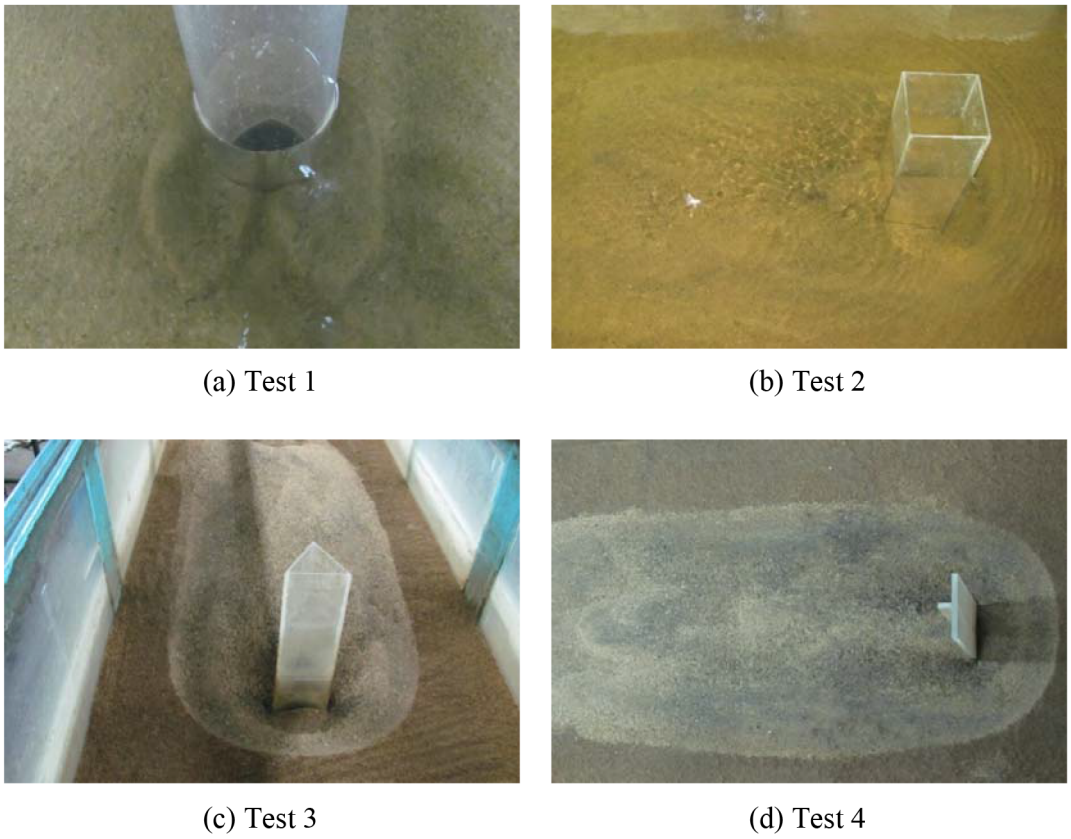

Figure 2. Scour affected zones around piers for tests 1–4.

Table 2. Magnitudes of geometrical scour parameters.

Test no.	b_e (cm)	d_{se} (cm)	l_{se} (cm)	w_{se} (cm)	a_{se} (cm^2)	v_{se} (cm^3)
1	11	9.2	46	53	2755	5835
2	15.5564	11.2	58	60	3031	9545
3	12.7020	9.6	48	49	2645	6842
4	11.0164	8.2	42	48	2251	4780

Note: Effective pier width b_e is the diameter of the smallest circumscribing circle of the pier; d_{se}, l_{se}, and w_{se} are the maximum equilibrium scour depth, length, and width, respectively.

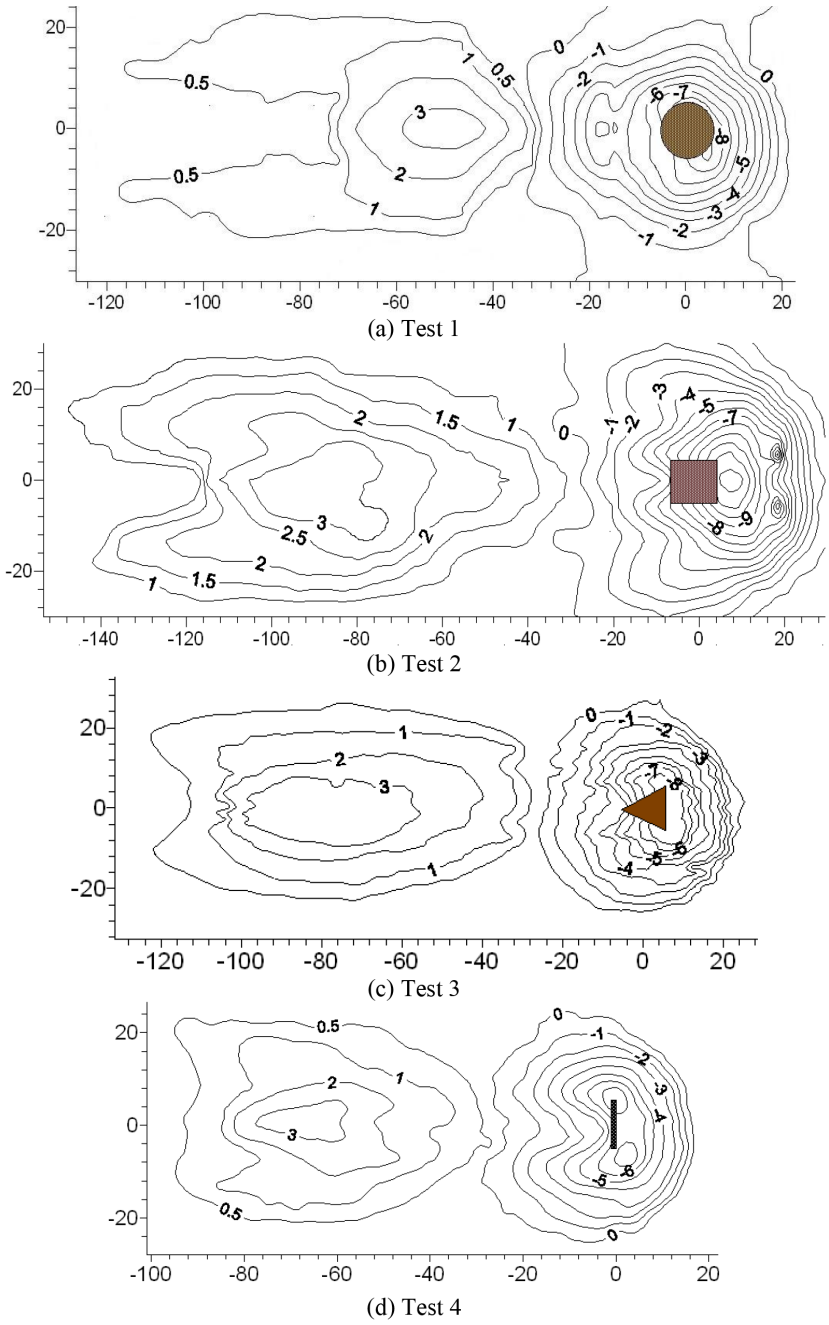

Figure 3. Contours of equilibrium scour holes for the tests 1–4 (units: cm).

3.1. Dimensional analysis

The magnitude that interests the designer for determining the pier depth is the maximum or equilibrium depth to be reached by the scouring process. For this reason, the quantitative study is limited to the maximum equilibrium depth d_{se} reached by the scour hole around the pier after sufficient time has elapsed to reach the equilibrium. Considering an isolated single pier in a rectangular tilting flume, where the flow is unidirectional and whose bed is made up of cohesionless sand particles, the equilibrium scour depth depends on the water

(density and viscosity), sand particles (density and median particle diameter), channel flow (flow depth, channel slope, and gravity), which is the section averaged velocity, and the geometry of the pier (a characteristic width, pier shape coefficient). For the circular pier the characteristic width b_c is same as the pier diameter [43].

The list of parameters is very long and some of them are, moreover, difficult to quantify, such as the particle size distribution, the grain form, and the cohesion of the bed materials. For this reason, the analysis was conducted mainly for the following restrictive conditions:

Bed material: the sediment is noncohesive and has a uniform size d_{50}.

Flow: flume is sufficiently wide so that the pier does not cause a significant contraction;

Pier: perfectly smooth surface.

The parameters that remain are:

- for the water: mass density ρ, kinematic viscosity ν, and gravitational acceleration g.
- for the bed material: median particle diameter d_{50} and its density ρ_s.
- for the flow: approaching flow depth h, and section averaged inflow velocity of the undisturbed flow U or the shear velocity u_* being equal to $\sqrt{ghS}$.
- for the pier: its characteristic pier width b_c.

The pier shape coefficient K_s is defined as the ratio of the scour depth for a particular pier shape to that for the circular pier. The circular shape is used for comparative purposes. Characteristic pier width, b_c which is equal to $b_e K_s$, can be considered a very important parameter since it takes into account both effective pier width b_e and pier shape coefficient K_s.

Therefore, the equilibrium scouring depth d_{se} depends on 8 parameters:

$$d_{se} = f\left(\rho, \nu, \rho_s, d_{50}, h, U, g, b_c\right) \tag{1}$$

The Vaschy–Buckingham π-theorem allows us to write:

$$\frac{d_{se}}{b_c} = f_0\left(\frac{u_* d_{50}}{\nu}, \frac{u_*^2}{\Delta g d_{50}}, \Delta, \frac{h}{b_c}, \frac{d_{50}}{b_c}\right) \tag{2}$$

The justification for the choice of the dimensionless groups is as follows:

- d_{se}/b_c : Experiments have clearly demonstrated that it was possible to relate scour depth to the characteristic diameter of the pier. This may be explained physically by the fact that scouring is due to the horseshoe-vortex system whose dimension is a function of the diameter of the pier [5].
- $u_* d_{50}/\nu, u_*^2/\Delta g d_{50}$: These are classical parameters in the study of bed load.
- h/b_c, d_{50}/b_c : These ratios relate the size and shape of the pier to that of the flow and of the sand particles.

Eq. (2) can be considerably simplified by the following considerations:

- The influence of kinematic viscosity ν is insignificant for a turbulent flow over rough beds [44].
- Shear velocity u_* was kept constant for all tests.

- In sediment–water interaction, the parameters g, ρ, and ρ_s were combined into one parameter, namely relative submerged weight, Δg, given by $\{(\rho_s/\rho)-1\}g$ [45,46]. The term Δ (=1.582) was also kept constant.

- The median particle diameter d_{50} and depth averaged inflow velocity U were kept constant for all 4 tests. Therefore, these terms can be neglected.

Thus, Eq. (2) can be written as

$$d_{se}/b_c = f_1\,(h/b_c) \tag{3}$$

It implies that the relative maximum equilibrium scour depth (d_{se}/b_c) can be expressed in nondimensional form as a function of inflow depth relative to characteristic pier width (h/b_c).

Similarly, the maximum equilibrium scour length relative to characteristic pier width (l_{se}/b_c) can be expressed as

$$l_{se}/b_c = f_2\,(h/b_c) \tag{4}$$

and for relative maximum equilibrium scour width (w_{se}/b_c),

$$w_{se}/b_c = f_3\,(h/b_c) \tag{5}$$

Multiplying Eqs. (4) and (5), the resulting equation can be regarded as planar surface area of the equilibrium scour hole (a_{se}/a_c) in nondimensional form where a_{se} and a_c, equal to πb_c^2, are the planar surface area of the equilibrium scour hole and characteristic area of the pier.

$$a_{se}/a_c = f_4\,(h/b_c) \tag{6}$$

Further, multiplying Eqs. (3), (4), and (5), a new nondimensional term known as volume of equilibrium scour hole relative to characteristic volume of pier (v_{se}/v_c) can be introduced, where v_{se} and v_c, equal to ha_c, are the volumes of equilibrium scour hole and immersed pier, respectively. Table 3 summarizes the values obtained for the nondimensional scour parameters for all tests.

$$v_{se}/v_c = f_5\,(h/b_c) \tag{7}$$

The influence of relative flow depth on the dimensionless scour depth was observed [5,43]. Sometimes some linear and empirical relations were proposed to correlate the geometrical scour parameters. Here an initiative was taken to find out those relations based on pier shape once again based on the experimental data.

Table 3. Magnitudes of nondimensional geometrical scour parameters.

Test no.	K_s (-)	h/b_c (-)	d_{se}/b_c (-)	l_{se}/b_c (-)	w_{se}/b_c (-)	a_{se}/a_c (-)	v_{se}/v_c (-)
1	1.00	1.14	0.80	4.05	4.54	6.43	1.26
2	1.21	0.66	0.60	3.07	3.09	2.81	0.69
3	1.04	0.94	0.72	3.65	3.95	4.59	0.96
4	0.89	1.27	0.86	4.33	4.95	8.16	1.26

3.2. Determination of pier shape coefficient

A dimensional analysis confirmed that the pier shape coefficient is a function of inflow depth relative to characteristic pier width h/b_c. The pier shape coefficient is plotted in Figure 4 as a function of relative inflow depth. From Figure 4, it can be revealed that the pier shape coefficient decreases with increasing relative inflow depth. A linear trendline is furnished in Figure 4, where the correlation coefficient (r) between the observations is 0.985; this implies an almost perfect positive correlation. The pier shape coefficient can be expressed as a function of relative inflow depth, as shown in Eq. (8).

$$K_s = -0.502\,(h/b_c) + 1.542 \tag{8}$$

The pier shape coefficient can be calculated using Eq. (8). The predicted values of the pier shape coefficient are estimated from Eq. (8). Figure 5 shows a comparison of observed and predicted values of the pier shape coefficient for tests 1–4. The ±5% deviation intervals are added as dashed lines. It can be seen from Figure 5 that the deviation between the predicted and measured data is in the range of –5% to 5%, which is the estimated pier shape coefficient; these results match the measured data very well.

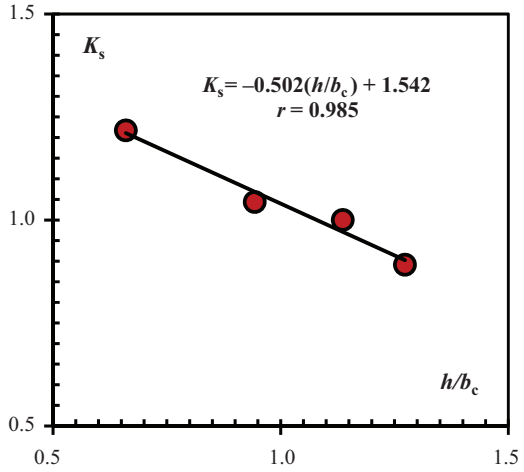

Figure 4. Variation in pier shape coefficient with relative inflow depth.

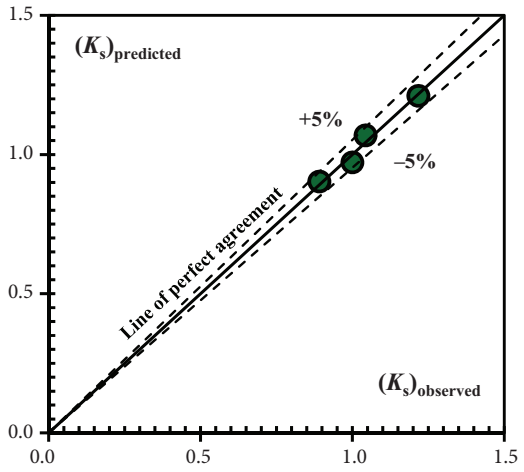

Figure 5. Comparison between observed and predicted values of pier shape coefficient.

3.3. Determination of scour depth

From the dimensional analysis it is observed that the equilibrium scour depth d_{se} is a function of inflow depth h. The dependency of nondimensional maximum equilibrium scour depth (d_{se}/b_c) on the ratio of approaching flow depth to characteristic pier width (h/b_c) is presented in Figure 6. At small h/b_c, the d_{se}/b_c increases with an increase in h/b_c. However, as h/b_c increases, d_{se}/b_c becomes almost independent of h/b_c. The results show good agreement with previous results [8,9], where it was stated that the influence of flow depth is insignificant for circular piers within the range of $1 < h/b_c < 3$. A linear trendline is furnished in Figure 6, where the correlation coefficient r is 0.987, which implies an almost perfect positive correlation. The scour depth can be expressed as a function of inflow depth, as shown in Eq. (9).

$$d_{se}/b_c = -0.364\,(h/b_c)^2 + 1.126\,(h/b_c) \tag{9}$$

The equilibrium scour depth can be computed using Eq. (9). The predicted values of equilibrium scour depth are calculated using Eq. (9). Figure 7 shows a comparison of observed and predicted values of equilibrium scour depth for tests 1–4. It may be seen from Figure 7 that Eq. (9) gives less than ±10% error for all the data. Therefore, the calculated scour depth matches the measured data very well.

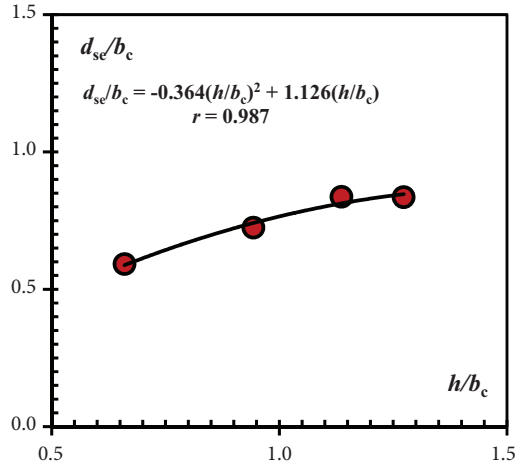

Figure 6. Variation in nondimensional maximum equilibrium scour depth with relative inflow depth.

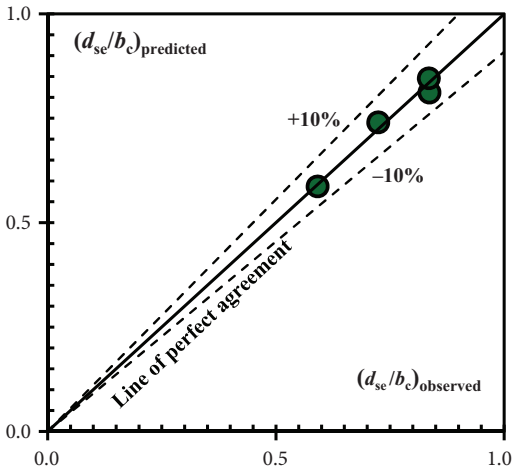

Figure 7. Comparison between observed and predicted values of nondimensional maximum equilibrium scour depth.

3.4. Determination of scour length

It is observed from the dimensional analysis that the equilibrium scour length l_{se} is a function of equilibrium scour depth d_{se}. The nondimensional maximum equilibrium scour length l_{se}/b_c is plotted as a function of nondimensional maximum equilibrium scour depth d_{se}/b_c in Figure 8, where it can be seen that the l_{se}/b_c increases with increasing d_{se}/b_c. A linear trendline is furnished in Figure 8, where the correlation coefficient r is 0.993, which implies an almost perfect positive correlation. The maximum equilibrium scour length can be expressed as a function of maximum equilibrium scour depth as shown in Eq. (10).

$$l_{se}/b_c = 5.065\,(d_{se}/b_c) \tag{10}$$

The maximum equilibrium scour depth may be determined using Eq. (10). The predicted values of l_{se} are calculated using Eq. (10). Figure 9 shows a comparison of observed and predicted values of nondimensional maximum equilibrium scour length l_{se}/b_c for tests 1–4. Figure 9 depicts that the deviation between the predicted and measured data is in the range of –20% to 20%, that is the calculated (predicted) l_{se} matches the measured (observed) data well.

3.5. Determination of scour width

As from the dimensional analysis, it is observed that the maximum equilibrium scour width w_{se} is a function of maximum equilibrium scour depth d_{se}. The maximum nondimensional equilibrium scour width w_{se}/b_c is plotted in Figure 10 as a function of maximum nondimensional maximum equilibrium scour depth d_{se}/b_c.

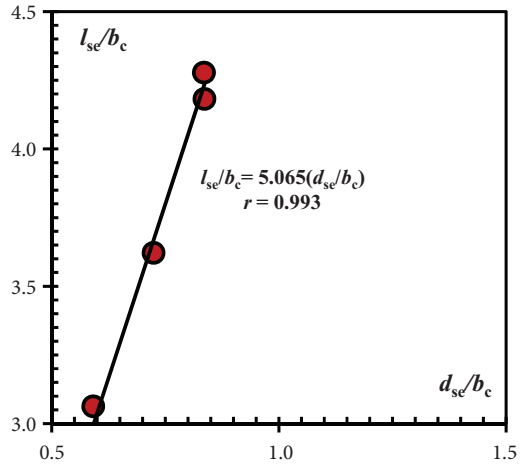

Figure 8. Variation in nondimensional maximum equilibrium scour length with nondimensional maximum equilibrium scour depth.

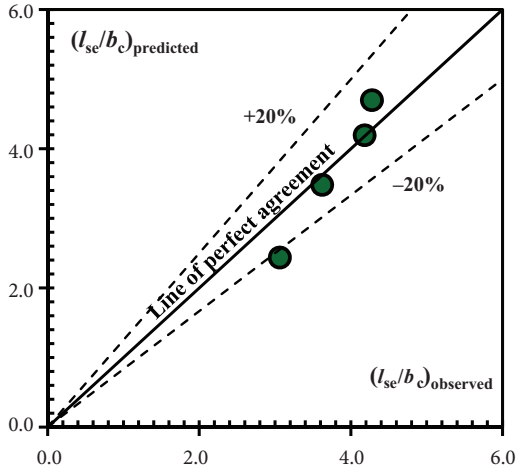

Figure 9. Comparison between observed and predicted values of nondimensional maximum equilibrium scour length.

From Figure 10 it can is observed that w_{se}/b_c increases with increasing d_{se}/b_c. A linear trendline is shown in Figure 10, where the correlation coefficient r between observations is 0.950, which indicates an almost perfect positive correlation. The w_{se} can be expressed as a function of d_{se}, as shown in Eq. (11).

$$w_{se}/b_c = 5.576\,(d_{se}/b_c) \tag{11}$$

The values of w_{se} may be calculated using Eq. (11). The predicted values of w_{se} are also computed from Eq. (11). Figure 11 shows a comparison of observed and predicted values of w_{se}. From Figure 11, it is observed that the deviation between the predicted and measured data is in the range of –15% to 15%, that is the calculated w_{se} is well within the measured data.

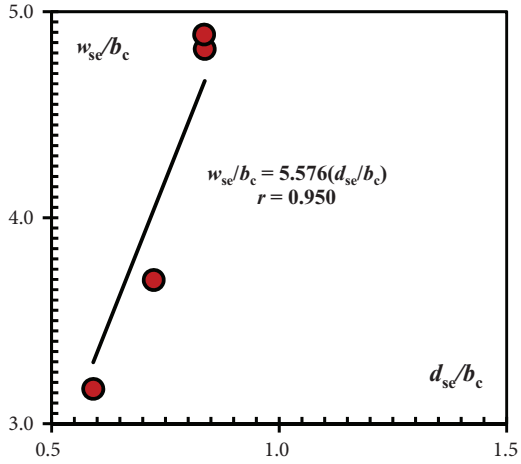

Figure 10. Variation in nondimensional maximum equilibrium scour width with nondimensional maximum equilibrium scour depth.

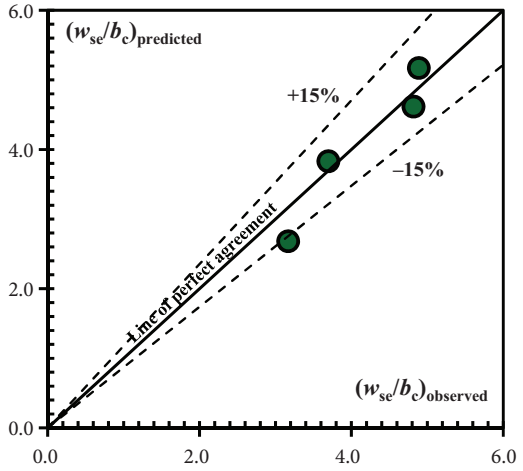

Figure 11. Comparison between observed and predicted values of nondimensional maximum equilibrium scour width.

3.6. Determination of scour area

The dimensional analysis also confirms that the planar surface area of the equilibrium scour hole a_{se} is a function of maximum equilibrium scour depth d_{se}. The maximum nondimensional equilibrium scour area a_{se}/b_c is plotted as a function of d_{se}/b_c in Figure 12, where it can be seen that the a_{se}/b_c increases with increasing d_{se}/b_c. An exponential trendline is furnished in Figure 12, having a correlation coefficient r of 0.999. The a_{se} can be expressed as a function of d_{se}, as shown in Eq. (12).

$$a_{se}/b_c = 0.242 \exp\{4.089\,(d_{se}/b_c)\} \tag{12}$$

Eq. (12) is not valid for an extreme case where d_{se} is equal to zero. Therefore, the relation between a_{se} and d_{se} can be rewritten as

$$a_{se}/b_c = 0.242\ [\{Exp\,(4.089 d_{se}/b_c)\} - 1] \tag{13}$$

The values of a_{se} may be computed using Eq. (13). The predicted values of a_{se} are also calculated using Eq. (13). Figure 13 shows a comparison of observed and predicted values for a_{se} in tests 1–4. It can be seen from Figure 13 that the deviation between the predicted and measured data is mostly in the range of –30% to 30%, which is the calculated a_{se} and matches the gauged data well.

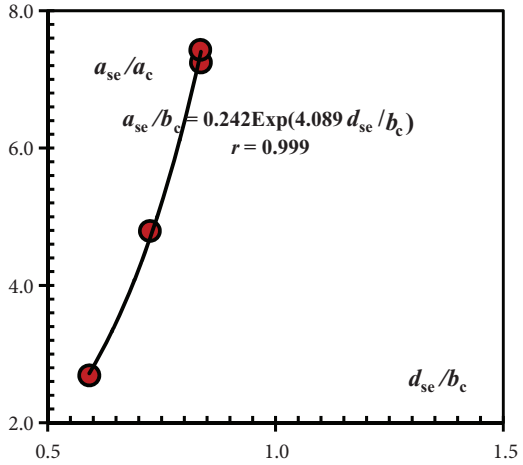

Figure 12. Variation in nondimensional equilibrium planner surface area with nondimensional maximum equilibrium scour depth.

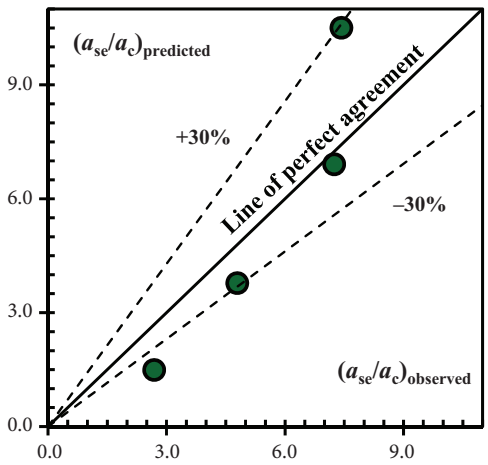

Figure 13. Comparison between observed and predicted values of nondimensional equilibrium planner surface area of scour hole.

3.7. Determination of scour volume

It is also observed from the dimensional analysis that the equilibrium scour volume v_{se} is a function of d_{se}. In Figure 14 the nondimensional equilibrium scour volume v_{se}/b_c is plotted as a function of d_{se}/b_c, where it can be observed that the scour volume increases with increasing scour depth at equilibrium scour condition. An exponential trend line is furnished in Figure 14, where the correlation coefficient r is 0.995, which implies an almost perfect positive correlation. The equilibrium scour volume v_{se} can be expressed as a function of maximum equilibrium scour depth d_{se} as shown in Eq. (14).

$$v_{se}/b_c = 0.161\exp\{2.461\,(d_{se}/b_c)\} \tag{14}$$

The values of v_{se} can be determined using Eq. (14). The predicted values of v_{se} may also be calculated using Eq. (14). Figure 15 shows a comparison of observed and predicted values of v_{se} for all tests. Figure 15 depicts that the deviation between the predicted and measured data is in the range of –25% to 25%, that is the predicted v_{se} matches the experimental data well.

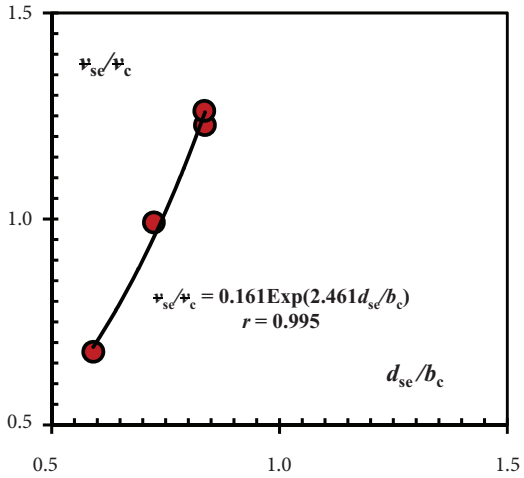

Figure 14. Variation in nondimensional equilibrium scour volume with nondimensional maximum equilibrium scour depth.

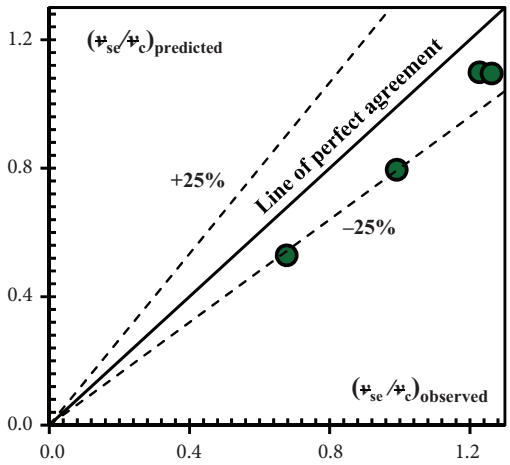

Figure 15. Comparison between observed and predicted values of nondimensional equilibrium scour volume.

4. Conclusions

Clear water scour tests were carried out on a circular pier, square pier, equilateral triangular pier, and a flat plate to measure the geometrical scour parameters in equilibrium condition. Some empirical relations were proposed based on the results. The main conclusions drawn from this paper are summarized below:

a) The pier shape coefficient is a function of inflow depth relative to characteristic flow shallowness h/b_c.

b) The relative equilibrium scour depth increases with increase in characteristic flow shallowness.

c) The dimensionless equilibrium scour length and width are found to increase with dimensionless equilibrium scour depth and thereby increase with characteristic flow shallowness.

d) Relative planar surface area and volume of equilibrium scour hole reveal an increase with characteristic flow shallowness.

e) Area and volume of scour hole varies exponentially with characteristic flow shallowness.

f) Simple new empirical relationships are proposed to evaluate equilibrium scour depth, length, width, surface area, and volume.

From this study, the experimental outcomes based on effective pier width may be used as a useful data bank not only to promote the related studies of scour parameters around different shaped piers, but also to validate the results obtained by numerical simulations.

5. Nomenclature

The following symbols are used in this paper:

a_c	$\left(\pi b_c^2\right)$ characteristic cross-sectional area of the pier or plate [L^2];	Q	discharge [$\mathrm{L}^3\,\mathrm{T}^{-1}$];
a_{se}	planar surface area of equilibrium scour hole [L^2];	r	correlation coefficient [—];
b	pier or plate width [L];	R_e	(UR/ν) flow Reynolds number [—];
b_c	$(b_e K_s)$ characteristic pier or plate width [L];	R_p	(Ub/ν) pier Reynolds number [—];
b_e	effective pier or plate width [L];	s	(ρ_s/ρ) relative density of sand [—];
d_s	scour depth measured at any instant from initial bed level [L];	u_c	critical velocity [LT^{-1}];
d_{se}	maximum equilibrium scour depth [L];	u_*	$\left(\sqrt{ghS}\right)$ shear velocity [LT^{-1}];
d_{16}	16% finer sand diameter [L];	U	section-averaged approaching flow velocity [LT^{-1}];
d_{50}	median diameter of sand [L];	v_c	(ha_c) characteristic volume of pier and plate below the water level [L^3];
d_{84}, d_{90}	84% and 90% finer sand diameter respectively [L];	v_{se}	volume of equilibrium scour hole [L^3];
F	$\left(U/\sqrt{gh}\right)$ Froude number of flow [—];	w_{se}	maximum equilibrium scour width [L];
g	gravitational acceleration [LT^{-2}];	ρ	mass density of water [ML^{-3}];
h	approaching flow depth [L];	ρ_s	mass density of sand [ML^{-3}];
K_s	ratio of the scour depths for any pier or plate to that for the circular pier [—];	Δ	$s-1$ [—];
l_{se}	maximum equilibrium scour length [L];	σ_g	$\left(\sqrt{d_{84}/d_{16}}\right)$ geometric standard deviation [—];
		ν	kinematic viscosity [$\mathrm{L}^2\,\mathrm{T}^{-1}$];
		φ	angle of repose [—];
		φ_r	dynamic angle of repose [—].

References

[1] Chabert J, Engeldinger P. Etude des Affouil-Lements antour des Piles des Ponts, Chanton, France: Laboratoire National d'Hydraulique; 1956.

[2] Laursen EM, Toch A. Scour around bridge piers and abutments, Vol. 4. Ames, Iowa, USA: Iowa Highway Research Board; 1956.

[3] Liu HK, Chang FM, Skinner MM. Effect of bridge constriction on scour and backwater. Report no. CER60HKL22, Civil Engineering Section, Colorado State Univ. Fort Collins, USA; 1961.

[4] Shen HW, Schneider VR, Karaki S. Local scour around bridge piers. J Hydraul Division 1969; 95: 1919–1940.

[5] Breusers HNC, Nicollet G, Shen HW. Local scour around cylindrical piers. J Hydraul Res 1977; 15: 211–252.

[6] Jain SC, Fischer EE. Scour around bridge piers at high Froude numbers. Report. no. FHWA-RD-79-104. Washington, DC, USA: Federal Highway Administration; 1979.

[7] Raudkivi AJ, Sutherland AJ. Scour at bridge crossings, Bulletin no. 54. Wellington, NZ, USA: National Roads Board Research Unit; 1981.

[8] Raudkivi AJ, Ettema R. Clear-water scour at cylindrical piers. J Hydraul Eng 1983; 109: 338–350.

[9] Raudkivi AJ. Functional trends of scour at bridge piers. J Hydraul Eng 1986; 112: 1–13.

[10] Froehlich DC. Local scour at bridge abutments, Proceedings National Conference on Hydraulic Engineering, NY, USA: ASCE; 1989. pp. 13–18.

[11] Breusers HNC, Raudkivi AJ. Scouring, IAHR Hydraulic Structures Design Manual, Vol. 2, Rotterdam, the Netherlands: AA Balkema; 1991.

[12] Melville BW. Local scour at bridge abutments. J Hydraul Eng 1992; 118: 615–631.

[13] Sumer BM, Fredsøe J. The Mechanics of Scour in the Marine Environment. Singapore: World Scientific; 2002.

[14] Abed L, Gasser, MM. Model study of local scour downstream bridge piers. In: Shen HW, Su ST, Wen F., editors, Proceedings of National Conference on Hydraulic Engineering. USA: ASCE; 1993. pp. 1738–1743.

[15] Richardson JR, Richardson EV. Practical method for scour prediction at bridge piers. Proceedings of National Conference on Hydraulic Engineering. Buffalo, NY, USA: ASCE; 1994. pp. 1–5.

[16] Dey S. Local Scour at Piers, Part 1: A Review of Development of Research. Int J Sediment Res 1997; 12: 23–44.

[17] Hoffmans GJCM, Verheij HC. Scour Manual, Rotterdam, the Netherlands: AA Balkema; 1997.

[18] Melville BW, Coleman SE. Bridge Scour. Colorado, USA: Water Resources Publications, LLC; 2000.

[19] Richardson EV, Davis SR. Evaluating Scour at Bridges. HEC18 FHWA NHI-001, Washington, DC, USA: Federal Highway Administration, US Department of Transportation; 2001.

[20] Barbhuiya AK, Dey S. Local scour at abutments: A review. Sadhana, Acad Proc Eng Sci 2004; 29: 449–476.

[21] Khwairakpam P, Ray SS, Das S, Das R, Mazumdar A. Scour hole characteristics around a vertical pier under clear water scour conditions. ARPN J Eng Appl Sci 2012; 7: 649–654.

[22] Melville BW. Scour at Bridge Sites, Report no. 104. Auckland, New Zealand: School of Engineering, University of Auckland; 1974.

[23] Anderson AG. Scour at bridge waterways – A review. US Department of Transportation. Office of Research and Development, USA: Environmental Design and Control Division; 1974.

[24] Hopkins GR, Vance RW, Kasraie B. Scour around bridge piers. Final reports FHWA-RD-78-163, FHWA-RD-75-56 (1975) and FHWA-RD-78-103 (1980). Washington, DC, USA: Federal Highway Administration; 1983.

[25] Jones JS. Comparison of prediction equations for bridge pier and abutment scour. Proceedings of Transportation Research Record. Second Bridge Engineering Conference, Vol. 2. Washington, DC, USA: Transportation Research Board; 1984. pp. 202–209.

[26] Johnson PA. Comparison of pier-scour equations using field data. J Hydraul Eng 1995; 121: 626–629.

[27] Mueller DS. Local scour at bridge piers in nonuniform sediment under dynamic conditions. PhD, Colorado State University, Fort Collins, CO, USA, 1996.

[28] Yanmaz AM. Time dependent analysis of clear water scour around bridge piers. PhD, Middle East Technical University, Ankara, Turkey, 1989.

[29] Melville BW. Local scour at bridge sites. Report no. 117. Auckland, New Zealand: School of Engineering, University of Auckland; 1975.

[30] Chiew YM, Melville BW. Local scour around bridge piers. J Hydraul Res 1987; 25: 15–26.

[31] Melville BW, Sutherland AJ. Design method for local scour at bridge piers. J Hydraul Eng 1988; 114: 1210–1226.

[32] Günyaktı A. Characteristics of alluvial streams and river training. Proceedings of Sediment Transport Technology, Vol. 2. UNESCO, Ankara, Turkey: General Directorate of State Hydraulic Works; 1989.

[33] Oliveto G, Hager WH. Temporal evolution of clear-water pier and abutment scour. J Hydraul Eng 2002; 128: 811–820.

[34] Oliveto G, Hager WH. Further results of time-dependent local scour at bridge elements. J Hydraul Eng 2005; 131: 97–105.

[35] Yanmaz AM, Köse O. Surface characteristics of scouring at bridge elements. Turkish J Eng Env Sci 2007; 31: 127–134.

[36] Das S, Das R, Mazumdar A. Vorticity and circulation of horseshoe vortex in equilibrium scour holes at different piers. J Inst Eng India Ser A 2014; 95: 109–115.

[37] Melville BW, Raudkivi AJ. Flow characteristics in local scour at bridge piers. J Hydraul Res 1977; 15: 373–380.

[38] Dey S, Bose SK, Sastry GLN. Clear water scour at circular piers: a model. J Hydraul Eng 1995; 121: 869–876.

[39] Das S, Das R, Mazumdar A. Circulation characteristics of horseshoe vortex in scour region around circular piers. Water Sci Eng 2013; 6: 59–77.

[40] Das S, Midya R, Das R, Mazumdar A. A study of wake vortex in the scour region around a circular pier. Int J Fluid Mech Res 2013; 40: 42–59.

[41] Dey S, Raikar RV. Characteristics of horseshoe vortex in developing scour holes at piers. J Hydraul Eng 2007; 133: 399–413.

[42] Das S, Das R, Mazumdar A. Comparison of characteristics of horseshoe vortex at circular and square piers. Res J Appl Sci Eng Tech 2013; 5: 4373–4387.

[43] Graf WH. Fluvial Hydraulics, Flow and Transport Processes in Channels of Simple Geometry. Great Britain: John Wiley and Sons; 2003.

[44] Yalin MS. Mechanics of sediment transport. Elmsford, NY, USA: Pergamon; 1977.

[45] Dey S, Debnath K. Sediment pickup on streamwise sloping beds. J Irrig Drain Eng 2001; 127: 39–43.

[46] Dey S, Raikar RV. Clear-water scour at piers in sand beds with an armor layer of gravels. J Hydraul Eng 2005; 133: 703–711.